Correction of interstitial water changes in calibration methods applied to XRF core-scanning major elements in long sediment cores: Case study from the South China Sea

Quan Chen, Catherine Kissel, Aline Govin, Zhifei Liu, Xin Xie

AGU PUBLICATIONS

Geochemistry, Geophysics, Geosystems

TECHNICAL REPORTS: METHODS

10.1002/2016GC006320

Key Points:
- Changes in interstitial water is the main factor to be corrected for XRF intensities in long cores
- A polynomial correction of interstitial water effect is proposed and applied to two existing XRF calibration methods
- The two improved calibrations proposed here are suited for correcting varying water contents in long sediment cores

Supporting Information:
- Supporting Information S1
- Data Set S1
- Data Set S2
- Data Set S3

Correspondence to:
Q. Chen,
quan.chen@hotmail.com

Citation:
Chen, Q., C. Kissel, A. Govin, Z. Liu, and X. Xie (2016), Correction of interstitial water changes in calibration methods applied to XRF core-scanning major elements in long sediment cores: Case study from the South China Sea, *Geochem. Geophys. Geosyst.*, *17*, 1925–1934, doi:10.1002/2016GC006320.

Received 24 FEB 2016
Accepted 12 APR 2016
Accepted article online 15 APR 2016
Published online 14 MAY 2016

Correction of interstitial water changes in calibration methods applied to XRF core-scanning major elements in long sediment cores: Case study from the South China Sea

Quan Chen[1,2], Catherine Kissel[2], Aline Govin[2], Zhifei Liu[1], and Xin Xie[1]

[1]State Key Laboratory of Marine Geology, Tongji University, Shanghai, China, [2]Laboratoire des Sciences du Climat et de l'Environnement/IPSL, CEA-CNRS-UVSQ, Université Paris Saclay, Gif-sur-Yvette Cedex, France

Abstract Fast and nondestructive X-ray fluorescence (XRF) core scanning provides high-resolution element data that are widely used in paleoclimate studies. However, various matrix and specimen effects prevent the use of semiquantitative raw XRF core-scanning intensities for robust paleoenvironmental interpretations. We present here a case study of a 50.8 m-long piston Core MD12-3432 retrieved from the northern South China Sea. The absorption effect of interstitial water is identified as the major source of deviations between XRF core-scanning intensities and measured element concentrations. The existing two calibration methods, i.e., normalized median-scaled calibration (NMS) and multivariate log-ratio calibration (MLC), are tested with this sequence after the application of water absorption correction. The results indicate that an improvement is still required to appropriately correct the influence of downcore changes in interstitial water content in the long sediment core. Consequently, we implement a new polynomial water content correction in NMS and MLC methods, referred as NPS and P_MLC calibrations. Results calibrated by these two improved methods indicate that the influence of downcore water content changes is now appropriately corrected. We therefore recommend either of the two methods to be applied for robust paleoenvironmental interpretations of major elements measured by XRF-scanning in long sediment sequences with significant downcore interstitial water content changes.

1. Introduction

Major element compositions of marine and lacustrine continuous sedimentary sequences have a great potential in a wide variety of research topics such as chronology, stratigraphy, sedimentology, paleoenvironment, and paleoceanography [*Norris and Röhl*, 1999; *Peterson et al.*, 2000; *Röhl and Abrams*, 2000; *Jaccard et al.*, 2005; *Mulitza et al.*, 2010; *Tjallingii et al.*, 2010; *Collins et al.*, 2013; *Govin et al.*, 2014]. Different approaches and methods have been used during the last years. The conventional geochemical analytical methods have high precision and accuracy. However, they are time consuming and, more importantly, they require a large number of destructive analyses to produce high-resolution downcore records of major element concentrations. X-ray fluorescence (XRF) core scanning techniques provide a nondestructive alternative to rapidly perform nearly continuous element measurements directly from the surface of untreated split sediment cores [*Jansen et al.*, 1998; *Kido et al.*, 2006; *Weltje and Tjallingii*, 2008]. The advantages of XRF core scanner over conventional destructive techniques led to its intensified use over the last decade.

The main drawback of XRF core-scanning (hereafter referred as "XRF-scanning") is that the element compositions are only semiquantitatively measured as element intensities and do not directly represent element concentrations in bulk sediments. Although XRF-scanning intensities are reported to be linearly correlated with element concentrations [e.g., *Jansen et al.*, 1998; *Böning et al.*, 2007], the linear relationship may be notably altered by various specimen and matrix effects [*Tjallingii et al.*, 2007; *Weltje and Tjallingii*, 2008; *Löwemark et al.*, 2011; *Hennekam and de Lange*, 2012; *Lyle et al.*, 2012; *Weltje et al.*, 2015]. Because these effects have different amplitudes depending on the element, even element ratios derived from XRF-scanning intensities may be strongly affected, inducing large uncertainties for paleoenvironmental interpretations. These features prevent the use of raw XRF-scanning element intensities or ratios from most paleoclimatic studies. Correction of these effects is, therefore, necessary for robust paleoenvironmental interpretations [e.g., *Tjallingii et al.*, 2007; *Hennekam and de Lange*, 2012; *Dang et al.*, 2015].

Most existing correction methods only partially correct the matrix and specimen effects in sediment sequences [e.g., *Kido et al*., 2006; *Tjallingii et al*., 2007; *Löwemark et al*., 2011; *Hennekam and de Lange*, 2012]. Besides "single-effect" corrections [e.g., *Löwemark et al*., 2011; *Hennekam and de Lange*, 2012], integrated calibration methods have been developed to take into account multiple effects. *Weltje and Tjallingii* [2008] proposed the log-ratio calibration equation (LRCE), which has recently been updated to a multivariate log-ratio calibration (MLC) that better accounts for the matrix effect and is able to predict bulk element concentrations [*Weltje et al*., 2015]. In parallel, *Lyle et al*. [2012] suggested a quick approach, the normalized median-scaled (NMS) method, to estimate sedimentary component concentrations in bulk sediments. The NMS method takes into account downcore density changes and differences in element efficiencies in producing characteristic X-ray.

XRF-scanning element intensities of long sedimentary sequences may exhibit an additional bias due to the downcore decrease in interstitial water induced by sediment compaction. So far, the NMS method is the only existing XRF calibration that has been applied on long sedimentary sequences, but a long-term bias was still observed in the NMS-calibrated $CaCO_3$ profile [*Lyle and Backman*, 2013].

In order to propose the most appropriate calibration methods to be applied in long sediment sequences, we use here a case study, performing element composition and XRF-scanning analyses on a 50.8 m-long core (MD12-3432) retrieved from the northern South China Sea. Through a quantitative comparison of XRF-scanning intensities and measured concentrations, we identify downcore changes in interstitial water content as the key factor influencing XRF-scanning intensities in this core. We then assess the performance of the existing correction and calibrations. Because they do not efficiently correct such water content changes, we implement them with a new correction, bringing us one step forward toward robust quantitative interpretations of major elements in long sedimentary sequences.

2. Material and Analytical Methods

Core MD12-3432 (19°16.88′ N, 116°14.52′ E, 2125 m water depth) was retrieved in 2012 onboard the R.V. *Marion Dufresne* during the French-Chinese CIRCEA cruise organized within the LIA-MONOCL framework [*Kissel et al*., 2012]. The core is 50.8 m long and it is located on the northern slope of the South China Sea, approximately 340 km offshore the Pearl River mouth. The sediment lithology is homogenously dominated by gray clays with several layers rich in organic matter, and the fractional porosity is higher in top sections than in lower sections [*Kissel et al*., 2012].

XRF core-scanning of major elements was performed on the working half of the core using an Avaatech XRF Core Scanner with standard procedures [*Xie et al*., 2014]. Each core section was removed from refrigeration at least 2 h before smoothing the surface and covering with a 4 μ thick ultralene film to avoid water condensation below the film. XRF-scanning data were collected every 1 cm over a 1.6 cm^2 area with a downcore slit size of 10 mm and a counting time of 30 s per sample. Major element (^{13}Al to ^{26}Fe) measurements were performed with a generator setting of 10 kV and a current of 0.2 mA, no filter was used.

In order to calibrate XRF-scanning intensities, 102 discrete bulk sediment samples were taken every 50 cm from the center of the working sections with a cubic container ($2 \times 2 \times 2$ cm). These discrete samples were first freeze-dried and weighted to calculate their dry bulk density. To quantitatively determine the major element composition of discrete sediment samples, wavelength dispersive XRF analyses (hereafter called "WD-XRF") were conducted. The dried bulk sediment was first manually ground in order to eliminate the potential influences of grain size. Then, 0.70000 ± 0.00008 g of sediment was melted with 7.0000 ± 0.0008 g of a fusion agent (mixture of lithium tetraborate and lithium metaborate) into a sample bead (3.7 cm diameter, 0.7 cm thick). The prepared sample beads were measured with a PANalytical AXIOS^{mAX} wavelength dispersive XRF spectrometer. Replicated analyses of the Chinese rock and sediment GSR6 and GSD15 standards were conducted every day at the beginning of the measurement runs to control the analytical precision and accuracy, and indicated a relative standard deviation lower than 1% and a relative accuracy lower than 6%. The use of complementary inductive coupled plasma atomic emission spectrometer (ICP-AES) analyses performed on additional discrete samples confirms the reliability of WD-XRF major element concentrations (see details in supporting information text S1).

Water content was measured at LSCE, France, by weighing 53 bulk sediment samples taken from the same horizons as WD-XRF samples, before and after drying. All other geochemical analyses were completed at the State Key Laboratory of Marine Geology (Tongji University), China. All data sets are available in supporting information.

3. Experimental Results

Noncalibrated XRF-scanning intensities (supporting information Data Set S1) and WD-XRF concentrations (supporting information Data Set S2) obtained in Core MD12-3432 are shown in Figure 1.

In this core, XRF-scanning Al, Si, and K intensities are relatively constant along the lower 25 m and progressively decrease upward along the upper 25 m of the core. Ca intensity continuously decreases upward, while Ti and Fe intensities remain relatively stable. WD-XRF concentrations do not exhibit such clear long-term trends, except for Si and Ca concentrations that slightly increase and decrease, respectively, upward along the core. WD-XRF concentrations of other elements are relatively stable throughout the core. Besides these long-term variations, rapid changes are observed both in XRF-scanning intensities and WD-XRF concentrations (despite their lower resolution) throughout the core. They are characterized by low intensities or concentrations of terrigenous elements (Al, Si, K, Ti, and Fe) and synchronous high Ca intensities or concentrations (Figure 1, yellow-shaded areas).

The linear relationship between XRF-scanning intensities and WD-XRF concentrations is not always sufficiently well-defined for direct linear calibration. The correlation coefficient (R^2), which is calculated using the WD-XRF data and XRF-scanning intensities from the same horizon, is high for Ca, moderate for K, Ti, and Fe, and low for Al and Si (Table 1).

To evaluate the differences between the between XRF-scanning and WD-XRF data measured at the same horizon, intensities are first scaled to the median concentration value of a given element, and relative differences (Δ) are then calculated. For element e at depth d, the relative difference ($\Delta_{e,d}$) is defined using equation (1):

$$\Delta_{e,d} = (I_{e,d}/I_{e,M} \times W_{e,M} - W_{e,d})/W_{e,d} \quad (1)$$

where $W_{e,M}$ and $I_{e,M}$ are the median values of all WD-XRF concentrations, and all XRF scanning intensities, respectively, of element e, $W_{e,d}$ and $I_{e,d}$ are WD-XRF concentration and the XRF scanning intensity, respectively, of element e at depth d.

These relative differences are also reported in Figure 1 for each element. They present diverse but notable long-term evolutions for the different elements. Indeed, while Δ_{Ti} and Δ_{Fe} are relatively constant throughout the core, Δ_{Al}, Δ_{Si}, and Δ_{K} are relatively high ($\sim$10%) in the lower 25 m of the core and decrease to negative values in the upper section. In contrast, Δ_{Ca} decreases by about 40% from the bottom to the top of the core. Such trends in relative differences suggest that specimen or matrix effects have affected the XRF-scanning intensities of Core MD12-343.

4. Assessing the Influence of Matrix and Specimen Effects in Core MD12-3432

The matrix effect corresponds to the scattering, absorption, and enhancement of XRF-scanning intensity caused by the presence of other elements. For instance, high Ca concentration absorbs the X-ray fluorescence of Ti and Fe, and causes excess excitation for K, resulting in artificially decreased Ti and Fe intensities and increased K intensities [*Kido et al*., 2006; *Böning et al*., 2007; *Kujau et al*., 2010]. In Core MD12-3432, the absence of a clear pattern in Δ records of K, Ti, and Fe in the intervals corresponding to Ca concentration peaks (Figure 1, yellow-shaded areas) indicates (1) that these short-term variations result from the relative dilution of biogenic material by terrigenous input and (2) that the Ca-content-related matrix effect has a very limited influence in Core MD12-3432.

Several sedimentary conditions are included in the so-called specimen effects. They were partly reduced in this case by smoothing the surface of split core before covering with the ultralene film and by the removal of low-quality data points induced by gaps and cracks within the sediment. Another possible specimen effect is the dry bulk density, which may increase the volume-normalized intensity of a given element. Indeed, higher dry bulk density increases the amount of all measured target elements and hence results in

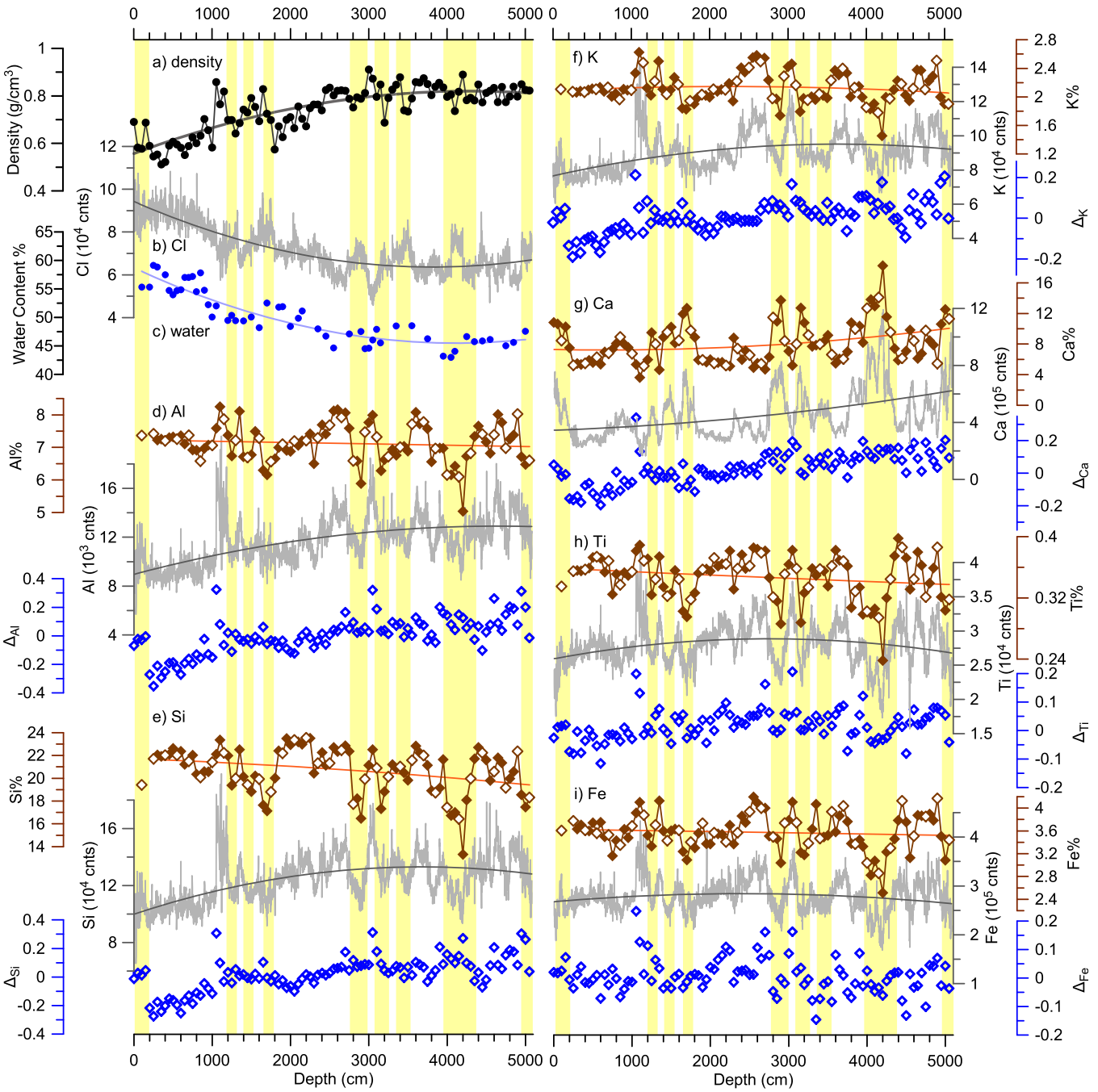

Figure 1. Downcore changes in XRF-scanning intensities and discrete WD-XRF element concentrations. (a) Dry bulk density (black dots); (b) XRF-scanning Cl intensity; (c) water content (blue dots); (d–i) WD-XRF element concentrations of both calibration (open brown diamonds) and evaluation data sets (solid brown diamonds), XRF-scanning intensities (gray lines), and relative differences (Δ, blue diamonds) of (d) Al, (e) Si, (f) K, (g) Ca, (h) Ti, and (i) Fe. Red and dark gray lines are the quadratic polynomial fits calculated from all discrete bulk sediment concentrations and XRF-scanning intensities, respectively. Yellow-shaded areas highlight short time intervals with high Ca concentrations (see sections 3 and 4).

higher intensities of all elements [*Lyle et al.*, 2012]. However, increased density may also reduce the transmission distance of X-ray, resulting in a decrease of analyzed sediment volume. In Core MD12-3432, the dry bulk density is significantly higher at the bottom than at the top of the core (Figure 1a), as commonly observed in long sediment cores because of the natural sediment compaction (e.g., in IODP sediment sequences [*Lyle et al*, 2012] and Calypso cores) and potential coring-induced stretching. Relatively constant XRF-scanning intensities and Δ values of heavy elements (Ti and Fe) throughout the core (Figures 1h and 1i) suggest here a limited influence of downcore changes in dry bulk density on XRF-scanning intensities in Core MD12-3432.

Table 1. Comparative Performance of Calibrations Based on the Independent Evaluation Data Set (Except for Regressions With Raw XRF-Scanning Intensities, see Footnote)[a]

		R^2						
	MSRE	Al	Si	K	Ca	Ti	Fe	Average
Raw intensities[b]		0.29	0.21	0.62	0.95	0.77	0.73	0.59
W_NMS[c]	0.00169	0.93	0.94	0. 92	0.98	0.84	0.66	0.88
W_MLC[c]	0.00183	0.81	0.96	0.91	0.99	0.68	0.49	0.81
NPS′[d]	0.00173	0.90	0.93	0.90	0.97	0.85	0.66	0.87
NPS[e]	0.00159	0.91	0.95	0.92	0.97	0.86	0.68	0.88
P_MLC[e]	0.00174	0.90	0.95	0.91	0.97	0.74	0.54	0.83

[a]The calibration results are evaluated using their mean squared relative errors (MSRE) and R^2 with respect to concentrations or relative element proportions of the WD-XRF evaluation data set.

[b]The R^2 values are calculated from linear regressions between raw XRF-scanning intensities and WD-XRF concentrations from the same horizon (102 horizons).

[c]The water attenuation correction defined by *Hennekam and de Lange* [2012] was applied to XRF-scanning intensities prior to running the NMS and MLC calibrations.

[d]NPS calibration with normalizing to unity rather than to WD-XRF sums (section 6.1).

[e]The polynomial correction proposed in this study was applied to account for downcore interstitial water changes in long sediment cores.

Water attenuation is the most discussed specimen effect for sedimentary sequences, because the presence of water absorbs X-ray energy, preferentially affecting light elements with weak fluorescence energies, in particular Al and Si [*Ge et al*., 2005; *Kido et al*., 2006; *Tjallingii et al*. 2007; *Hennekam and de Lange*, 2012]. The water attenuation effect can derive from the water film formed under the covering foil or from downcore changes in the water content, which both need to be scrutinized.

In marine sediment cores, XRF-scanning Cl intensity can be used as a proxy for water content [*Kido et al*., 2006; *Tjallingii et al*. 2007; *Hennekam and de Lange*, 2012]. In Core MD12-3432, Cl intensity decreases downcore (Figure 1b), similarly to the low-resolution water content decrease (Figure 1c) and in opposition with the dry bulk density increase (Figure 1a). Long-term changes in Cl intensity hence mainly represent variations in interstitial water content in this core. As core stretching is limited with the new coring device onboard R/V *Marion Dufresne* (we checked with other analyses that it does not exceed the top 1.5 m in Core MD12-3432), these simultaneous variations suggest that water content is gradually reduced downward due to natural sediment compaction. Therefore, the long-term trends of element intensities and Δ values of lighter elements (Al, Si, K, and Ca), compared to the stability of heavier elements (Ti and Fe), most likely result from the increasing water contents in upper sections (Figure 1). In addition, coeval short-term increases in Cl intensity and decreases in dry bulk density (Figure 1, yellow-shaded areas) indicate that these short-term Cl changes predominantly represent variations in interstitial water content in this study (and not changes in the thickness of the water film as reported by *Hennekam and de Lange* [2012]). Coeval with low XRF intensity values for all terrigenous elements, independently from their atomic mass, these short-term water content increases have, however, a very limited impact on XRF-scanning intensities. Therefore, the XRF-scanning intensities in this study remain mainly affected by the long-term downcore decrease in interstitial water.

5. Calibration Methods and Results

In order to determine which calibration method is the most suitable for long sedimentary sequences with large downcore water content variations, we tested on Core MD12-3432 the two most recent integrated calibrations, the NMS [*Lyle et al*., 2012; *Lyle and Backman*, 2013], and MLC [*Weltje et al*., 2015]. To test the most up-to-date calibration methods accounting for the water attenuation effect, we applied the correction of water absorption effect defined by *Hennekam and de Lange* [2012], prior to running the NMS and MLC calibrations (see calculation details in supporting information text S2). Hereafter, we refer to these water-corrected calibration methods as W_NMS and W_MLC. The effect of this water correction on NMS- and MLC-calibrated results is evaluated in supporting information, text S2.4.

Thirty-four of the samples analyzed by WD-XRF (hereafter called "calibration dataset") are used to convert XRF-scanning intensities into calibrated concentrations and relative proportions of six major elements (Al, Si, K, Ca, Ti, and Fe). The remaining 68 WD-XRF samples (hereafter called "evaluation dataset") are used to evaluate the quality of tested calibrations. The evaluation of calibrations is therefore done independently

from the calibration data set. Several tries with different numbers of calibration versus evaluation data points yielded very similar results (not shown).

The mean squared relative error (MSRE) of elements is used below to quantitatively compare the performance of different calibrations. MSRE is calculated following equation (2):

$$\mathrm{MSRE} = \frac{1}{nD}\sum_{d=1}^{n}\sum_{e=1}^{D}\delta_{e,d} \tag{2}$$

where n and D are the number of measured horizons and calibrated elements, respectively; $\delta_{e,d}$ is the relative error of element e at depth d defined as:

$$\delta_{e,d} = (C_{e,d} - W_{e,d})/W_{e,d} \tag{3}$$

where $C_{e,d}$ is the calibrated value of element e at depth d, $W_{e,d}$ is the WD-XRF concentration of element e at depth d.

5.1. Normalized Median-Scaled Calibration (NMS) Applied to This Case Study

The NMS calibration [*Lyle et al*., 2012; *Lyle and Backman*, 2013] builds a reasonable model to quickly estimate the concentrations of sedimentary components in bulk sediments (i.e., Al_2O_3, SiO_2, K_2O, $CaCO_3$, TiO_2, and Fe_2O_3 in this study) from a limited number of discrete measurements (see supporting information text S2.2 for the detailed procedure). Note that it was performed here on the water-corrected XRF-scanning intensities of Core MD12-3432 (see above). The W_NMS-calibrated component concentrations were then converted to element concentrations (e.g., %Ca for Ca) in bulk sediments to simplify the comparison to element percentages provided by the MLC method (section 5.2).

The W_NMS calibration significantly improves R^2 values, in particular for Al%, Si%, and K% (Table 1), compared to the direct linear correlation of raw XRF-scanning intensities with WD-XRF concentrations. Although, in first approximation, the W_NMS-calibrated Al%, Ti%, ln(Al/Ti), and ln(Al/K) follow the variations shown by the WD-XRF evaluation data, long-term deviations are still observed for these records (Figures 2a–2d). Indeed, W_NMS-calibrated ln(Al/Ti), ln(Al/K), and Al% are lower than those in the evaluation data set in the upper sections of the core, while they are higher in the bottom part (Figures 2a–2c). Their relative differences hence exhibit an upward decreasing long-term trend. The Ti%, as well as the associated relative differences, exhibits an opposite relationship (Figure 2d). These deviations are similar to those observed in raw XRF-scanning intensities (Figure 1) and in carbonate content of IODP core U1338 [*Lyle and Backman*, 2013]. As water preferentially absorbs weak fluorescence energies of light elements, these deviations suggest that the impact of water attenuation effect is not appropriately corrected.

5.2. Multivariate Log-Ratio Calibration (MLC) Applied to This Case Study

Derived from the LRCE [*Weltje and Tjallingii*, 2008], the MLC method [*Weltje et al*., 2015] is a mathematically rigorous method designed to calibrate element concentrations in bulk sediments (see details in supporting information text S2.3). The use of centered log-ratios and partial least squares regression allows MLC to better account for the matrix effect [*Weltje et al*., 2015].

The MLC was performed on water-corrected XRF-scanning intensities of Core MD12-3432 (referred to as W_MLC) using the XELERATE software available online (www.ascar.nl), choosing Ca as common denominator of all log-ratios (i.e., ln(Al/Ca), ln(Si/Ca), ln(K/Ca), ln(Ti/Ca), ln(Fe/Ca), mean $R^2 = 0.97$). To ensure the comparison with other calibration methods, the W_MLC was forced to perform the calibration with the entire WD-XRF calibration data set. As bulk concentrations are not predicted at the moment by the software, the calibrated relative proportions provided by the XELERATE software were used here to evaluate its performance.

W_MLC-calibrated relative proportions of elements also show strong linear correlations to the WD-XRF evaluation data set. The R^2 value of MLC-calibrated Al% and Si% reach 0.81 and 0.96, respectively (Table 1), but the MSRE is larger than that of the W_NMS calibration (Table 1). Similarly to W_NMS-calibrated results, the W_MLC-calibrated Al%, ln(Al/Ti), and ln(Al/K) are lower than the evaluation data points in the top sections of the core (Figures 2e–2g). These differences between W_MLC-calibrated and WD-XRF results, which are also illustrated by the long-term trends in relative differences (Figures 2e–2h), suggest that the water attenuation effect is not appropriately corrected here either.

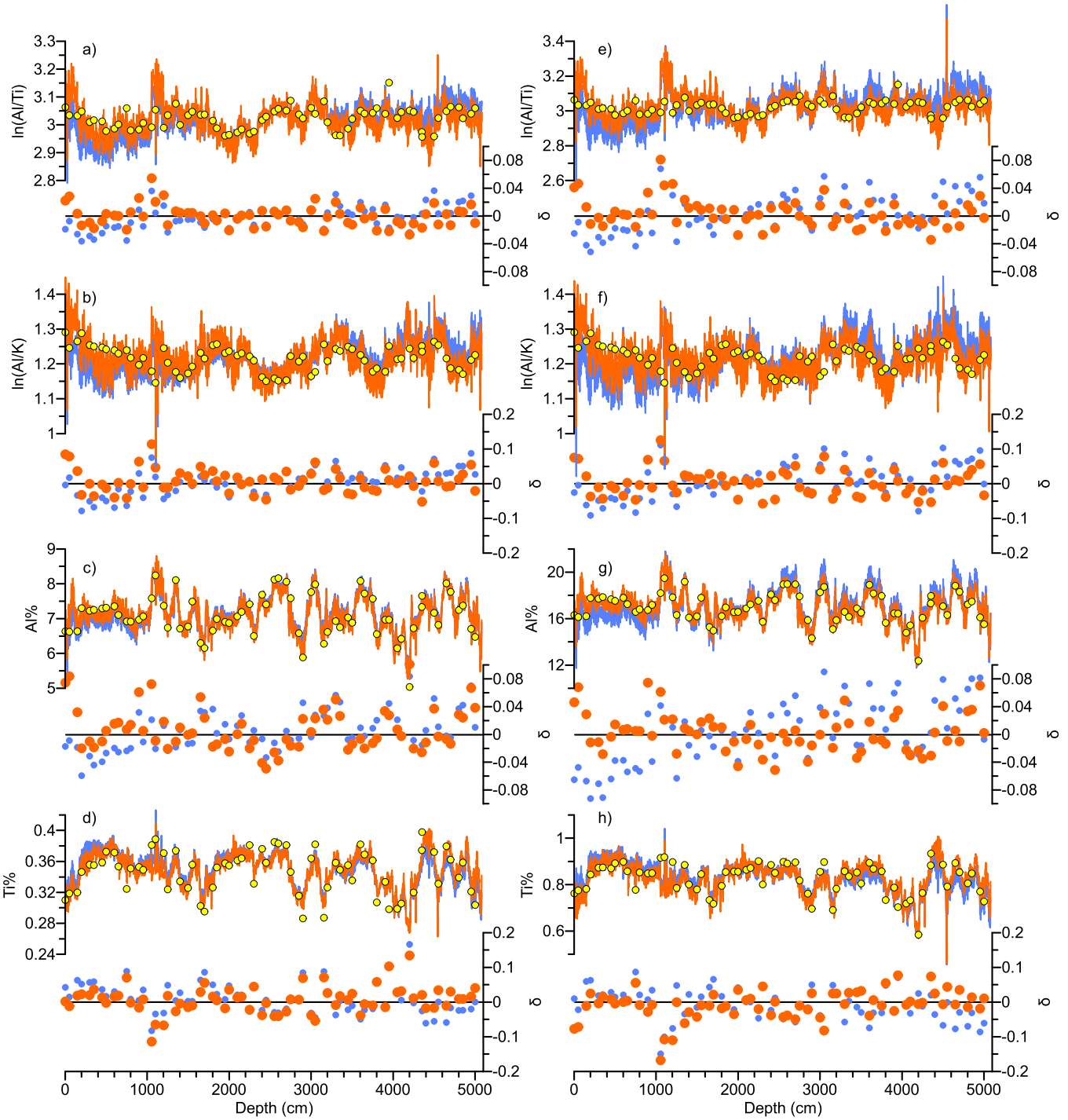

Figure 2. Results of the improved calibrations. (a–d): NPS-calibrated results (orange lines) and W_NMS results (blue lines), together with their relative errors (orange and small blue dots, respectively), are shown in Figure 2a (left) ln(Al/Ti), (b) ln(Al/K), and concentrations of (c) Al, (d) Ti. (e–h): P_MLC-calibrated results (orange lines) and W_MLC results (blue lines), together with their relative errors (orange and small blue dots, respectively), are shown in Figure 1e (right) ln(Al/Ti), (f) ln(Al/K), and relative proportions of (g) Al, (g) Ti. WD-XRF evaluation data are plotted as yellow dots.

5.3. Ability of Existing Methods to Account for Interstitial Water Changes in This Case

The observed deviations between WD-XRF on one hand, and W_NMS-calibrated (section 5.1) or W_MLC-calibrated (section 5.2) results on the other hand, indicate that none of these two methods sufficiently accounts for downcore interstitial water changes, even after applying the water absorption correction to

raw intensities as proposed by *Hennekam and de Lange* [2012] (also see supporting information text S2.4).

The correction proposed by *Hennekam and de Lange* [2012], which was developed from three short sediment sequences where the effect of water absorption mainly derives from changes in the water film thickness, is indeed not sufficiently robust when water content variations are predominantly driven by interstitial water changes due to downcore sediment compaction as in this case study (see section 4). A more appropriate correction is therefore required for long sediment cores with large interstitial water content changes.

6. Improved Correction and Its Implementation in XRF Calibrations

The major effect of the downcore decrease of interstitial water content on XRF-scanning intensities, expressed in this case study as a downcore increasing trend in light elements, suggests that it can be removed by correcting the long-term trend of XRF-scanning intensities. A quadratic polynomial fit, which is the simplest polynomial that best describes such downcore water content changes, is selected here to subtract this long-term variation. A simple polynomial subtraction directly applied to XRF-scanning intensities is not appropriate because gradual changes in XRF-scanning intensities and log-ratios incorporate not only the influence of water content changes but also long-term environmental signals. Therefore, the fit of the quadratic polynomial evolution of XRF-scanning intensities and log-ratios to that of WD-XRF data in the calibration data set allows to correct the gradual water content changes and to preserve environmental signals.

The details of correction and calibration procedures are summarized in the following sections and fully described in supporting information text S3.

6.1. Normalized Polynomial-Scaled Calibration (NPS) Applied to This Case Study

The normalized polynomial-scaled calibration (NPS) proposed here, which is derived from the NMS calibration (section 5.1), also includes three steps: (1) scaling the raw XRF-scanning intensities to the range of WD-XRF component concentrations using quadratic polynomial fits (instead of median values as in NMS), (2) normalizing the sum of scaled intensities to that of WD-XRF concentrations (instead of unity as in NMS), which remains below 90% in Core MD12-3432 due to the presence of organic matter and other components not considered here, and (3) calibrating the normalized polynomial-scaled data to WD-XRF concentrations using linear regression equations. The calibrated component concentrations were then transformed to element concentrations to simplify the comparison with other methods.

In this case study, we first tested the normalization to unity (NPS') for comparison with NPS. Element concentrations calibrated with both normalizations are highly correlated with WD-XRF concentrations (Table 1). Although concentrations of excluded components (e.g., organic matter, Mg, Na) vary between 11 and 18% only, i.e., have a small range of variations (smaller than 7%), the NPS-calibrated results show smaller MSRE and higher mean R^2 than NPS'-calibrated ones. These results indicate that normalizing to interpolated WD-XRF sums in the NPS method (instead of to unity in NMS) better accounts for variations in sedimentary components that are not included in the calibration. This feature strongly improves the applicability of the NPS method, in particular for sediments in which organic matter is abundant.

NPS presents the smallest calibration error (smallest MSRE value) among all the evaluated methods in this case study (Table 1). The downcore variations in NPS-calibrated ln(Al/Ti) and ln(Al/K) (Figures 2a and 2b), as well as in Al% and Ti% (Figures 2c and 2d), better correlate to WD-XRF data points than W_NMS-calibrated results. The relative errors of NPS results randomly distributed around zero with no long-term variations visible anymore (Figures 2a–2d). These results show that the polynomial scaling in NPS empirically and reasonably removes the influence of downcore interstitial water content decrease. Therefore, the NPS method better accounts for the influence of downcore water content changes than W_NMS and it calibrates XRF-scanning intensities to robust individual element concentrations in long sediment cores with large downcore water.

More discrete geochemical analyses are probably required in the NPS method compared to NMS in order to build robust reference polynomial regressions and to reduce uncertainties derived from interpolating

reference sums. Small errors in NPS-calibrated results (Table 1 and Figure 2) suggest that 34 discrete measurements are sufficient in this case study.

Although, in this study, small relative errors of NPS-calibrated ln(Al/Ti) and ln(Al/K) (Figure 2a and 2b) indicate a good preservation of relative element proportions, the latter may be altered during calibration due to the fact that the linear regressions of the NPS calibration are performed on single elements and not on element ratios [e.g., *Aitchison and Egozcue*, 2005]. Such data evaluation is therefore strongly recommended after performing the NPS calibration.

6.2. Polynomial-Corrected Multivariate Log-Ratio Calibration (P_MLC) Applied to This Case Study

In the P_MLC calibration, a polynomial correction is first performed on the raw XRF-scanning intensities in the log-ratio space. The standard MLC [*Weltje et al*., 2015] is then performed on the polynomial-corrected intensities using the XELERATE software (section 5.2). In this case study, Ca was again chosen as the common denominator.

P_MLC-calibrated relative proportions correlate well with WD-XRF concentrations (mean R^2 of 0.83) (Table 1). Compared to the W_MLC method, P_MLC produces smaller MSRE and improves the correlation for Al, Ti, and Fe (Table 1). The downcore variations in P_MLC-calibrated ln(Al/Ti) and ln(Al/K) (Figures 2e and 2f), as well as in Al% and Ti% (Figures 2g and 2h), better correlate to WD-XRF data points than for W_MLC results. Relative errors of P_MLC results randomly distribute around zero without the long-term trend previously observed in XRF-scanning intensities (Figures 1d and 1h) and in W_MLC-calibrated results (Figures 2e–2h). Altogether, these results indicate that the P_MLC method efficiently corrects the effect of water content changes on XRF-scanning intensities and provides more accurate relative element proportions than the W_MLC method.

Therefore, the polynomial-correction in the log-ratio space reasonably corrects the influence of downcore interstitial water content changes on XRF-scanning intensities. Based on the mathematically rigorous LRCE [*Weltje and Tjallingii*, 2008] and MLC [*Weltje et al*., 2015] calibrations, the P_MLC method respects the mathematical constraints imposed by compositional data [*Aitchison and Egozcue*, 2005] and preserves in particular the relative proportions of elements.

7. Conclusions

The comparison of XRF-scanning intensities and WD-XRF major element concentrations in a 50.8 m-long sediment Core MD12-3432 used as a case study shows that the downcore decrease in interstitial water content in long sediment cores is the main source of deviations in XRF-scanning intensities. Previously proposed calibration approaches (W_NMS and W_MLC) fail to appropriately account for this influence of large downcore interstitial water changes and need to be improved.

We propose a quadratic polynomial correction to empirically remove the effect of downcore interstitial water content changes on XRF-scanning intensities and implement it in the two existing integrated NMS and MLC calibrations. From this case study, we show that the two improved NPS and P_MLC calibrations are so far the most appropriate methods to correct the effect of interstitial water content changes on XRF-scanning intensities and provide accurate high-resolution concentrations of major elements derived from XRF core scanning in long sediment cores.

We strongly recommend testing and applying either the NPS or the P_MLC method for robust paleoenvironmental interpretations based on major element contents in long sediment cores (e.g., Calypso cores collected with the R/V *Marion Dufresne*, and long-drilled sequences taken as part of the International Ocean Discovery Program).

Acknowledgments

We greatly appreciate the constructive suggestions and comments from three reviewers which helped us to improve this manuscript. We are grateful to all the crew of the R.V. *Marion Dufresne*, to IPEV team, and to the on-board scientific party of the CIRCEA cruise. The work is implemented under the France-China framework of LIA-MONOCL (Laboratoire International Associé: MONsoon, Ocean and CLimate). The study is financially supported by the National Natural Science Foundation of China (91128206 and 91528304) and by the CNRS funds to the LIA-MONOCL. Q. C is funded by the China Scholarship Council for his research stay in France. This is LSCE contribution number 5728. Analytical results are provided as supporting information Data Set S1–S3.

References

Aitchison, J., and J. J. Egozcue (2005), Compositional data analysis: Where are we and where should we be heading?, *Math. Geol.*, *37*(7), 829–850, doi:10.1007/s11004-005-7383-7.

Böning, P., E. Bard, and J. Rose (2007), Toward direct, micron-scale XRF elemental maps and quantitative profiles of wet marine sediments, *Geochem. Geophys. Geosyst.*, *8*, Q05004, doi:10.1029/2006GC001480.

Collins, J. A., A. Govin, S. Mulitza, D. Heslop, M. Zabel, J. Hartmann, U. Röhl, and G. Wefer (2013), Abrupt shifts of the Sahara–Sahel boundary during Heinrich stadials, *Clim. Past*, *9*(3), 1181–1191, doi:10.5194/cp-9-1181-2013.

Dang, H., Z. Jian, C. Kissel, and F. Bassinot (2015), Precessional changes in the western equatorial Pacific Hydroclimate: A 240 kyr marine record from the Halmahera Sea, East Indonesia, *Geochem. Geophys. Geosyst.*, *16*, 148–164, doi:10.1002/2014GC005550.

Ge, L., W. Lai, and Y. Lin (2005), Influence of and correction for moisture in rocks, soils and sediments on in situ XRF analysis, *X-Ray Spectrom.*, *34*(1), 28–34, doi:10.1002/xrs.782.

Govin, A., C. Chiessi, M. Zabel, A. Sawakuchi, D. Heslop, T. Hörner, Y. Zhang, and S. Mulitza (2014), Terrigenous input off northern South America driven by changes in Amazonian climate and the North Brazil Current retroflection during the last 250 ka, *Clim. Past*, *10*(2), 843–862, doi:10.5194/cp-10-843-2014.

Hennekam, R., and G. de Lange (2012), X-ray fluorescence core scanning of wet marine sediments: Methods to improve quality and reproducibility of high-resolution paleoenvironmental records, *Limnol. Oceanogr. Methods*, *10*(12), 991–1003, doi:10.4319/lom.2012.10.991.

Jaccard, S. L., G. H. Haug, D. M. Sigman, T. F. Pedersen, H. R. Thierstein, and U. Röhl (2005), Glacial/interglacial changes in subarctic North Pacific stratification, *Science*, *308*(5724), 1003–1006, doi:10.1126/science.1108696.

Jansen, J. H. F., S. J. Van der Gaast, B. Koster, and A. J. Vaars (1998), CORTEX, a shipboard XRF-scanner for element analyses in split sediment cores, *Mar. Geol.*, *151*(1–4), 143–153, doi:10.1016/S0025-3227(98)00074-7.

Kido, Y., T. Koshikawa, and R. Tada (2006), Rapid and quantitative major element analysis method for wet fine-grained sediments using an XRF microscanner, *Mar. Geol.*, *229*(3–4), 209–225, doi:10.1016/j.margeo.2006.03.002.

Kissel, C., Z. Jian, and H. Leau (2012), MD190-CIRCEA cruise report, *Ref. OCE/2012/01*, Institut polaire français - Paul Émile Victor (IPEV), Brest.

Kujau, A., D. Nürnberg, C. Zielhofer, A. Bahr, and U. Röhl (2010), Mississippi River discharge over the last ~560,000 years: Indications from X-ray fluorescence core-scanning, *Palaeogeogr. Palaeoclimatol. Palaeoecol.*, *298*(3–4), 311–318, doi:10.1016/j.palaeo.2010.10.005.

Löwemark, L., H. F. Chen, T. N. Yang, M. Kylander, E. F. Yu, Y. W. Hsu, T. Q. Lee, S. R. Song, and S. Jarvis (2011), Normalizing XRF-scanner data: A cautionary note on the interpretation of high-resolution records from organic-rich lakes, *J. Asian Earth Sci.*, *40*(6), 1250–1256, doi:10.1016/j.jseaes.2010.06.002.

Lyle, M., and J. Backman (2013), Data report: Calibration of XRF-estimated $CaCO_3$ along the Site U1338 splice, in *Proceedings of IODP*, *320/321*, edited by H. Pälike et al., Integrated Ocean Drill. Program Manage. Int., Inc., Tokyo, 349–360, doi:10.2204/iodp.proc.320321.205.2013.

Lyle, M., A. O. Lyle, T. Gorgas, A. Holbourn, T. Westerhold, E. Hathorne, K. Kimoto, and S. Yamamoto (2012), Data report: Raw and normalized elemental data along the Site U1338 splice from X-ray fluorescence scanning, in *Proceedings of IODP, 320/321*, edited by H. Pälike et al., Integrated Ocean Drill. Program Manage. Int., Inc., Tokyo, doi:10.2204/iodp.proc.320321.203.2012.

Mulitza, S., et al. (2010), Increase in African dust flux at the onset of commercial agriculture in the Sahel region, *Nature*, *466*(7303), 226–228, doi:10.1038/nature09213.

Norris, R. D., and U. Röhl (1999), Carbon cycling and chronology of climate warming during the Palaeocene/Eocene transition, *Nature*, *401*(6755), 775–778, doi:10.1038/44545.

Peterson, L. C., G. H. Haug, K. A. Hughen, and U. Röhl (2000), Rapid Changes in the Hydrologic Cycle of the Tropical Atlantic During the Last Glacial, *Science*, *290*(5498), 1947–1951, doi:10.1126/science.290.5498.1947.

Röhl, U., and L. J. Abrams (2000), High-resolution, downhole, and nondestructive core measurements from sites 999 and 1001 in the Caribbean Sea: Application to the late Paleocene thermal maximum, in *Proceedings of ODP Science Results*, edited by R. M. Leckie et al. pp. 191–203, Ocean Drill. Program, College Station, Tex.

Tjallingii, R., U. Röhl, M. Kölling, and T. Bickert (2007), Influence of the water content on X-ray fluorescence core-scanning measurements in soft marine sediments, *Geochem. Geophys. Geosyst.*, *8*, Q02004, doi:10.1029/2006GC001393.

Tjallingii, R., K. Stattegger, A. Wetzel, and P. Van Phach (2010), Infilling and flooding of the Mekong River incised valley during deglacial sea-level rise, *Quat. Sci. Rev.*, *29*(11–12), 1432–1444,. doi:10.1016/j.quascirev.2010.02.022.

Weltje, G. J., and R. Tjallingii (2008), Calibration of XRF core scanners for quantitative geochemical logging of sediment cores: Theory and application, *Earth Planet. Sci. Lett.*, *274*(3–4), 423–438, doi:10.1016/j.epsl.2008.07.054.

Weltje, J. G., R. M. Bloemsma, R. Tjallingii, D. Heslop, U. Röhl, and W. I. Croudace (2015), Prediction of Geochemical Composition from XRF Core Scanner Data: A New Multivariate Approach Including Automatic Selection of Calibration Samples and Quantification of Uncertainties, in *Micro-XRF Studies of Sediment Cores: Applications of a non-destructive tool for the environmental sciences*, edited by W. I. Croudace and G. R. Rothwell, pp. 507–534, Springer, Dordrecht, Netherlands, doi:10.1007/978-94-017-9849-5_21.

Xie, X., H.-B. Zheng, and P.-J. Qiao (2014), Millennial climate changes since MIS 3 revealed by element records in deep-sea sediments from northern South China Sea, *Chin. Sci. Bull.*, *59*(8), 776–784, doi:10.1007/s11434-014-0117-9.